Geoenvironmental Disasters

RESEARCH

Open Access

Investigation of landslide triggers on Mount Oku, Cameroon, using Newmark displacement and cluster analysis

D. L. W. Djukem[1], A. Braun[2*], X. Fan[1], A. S. L. Wouatong[3], T. M. Fernandez-Steeger[2] and H. B. Havenith[4]

Abstract

Background The landslide inventory of the western flank of Mount Oku, Cameroon, includes spreads or complex landslides, indicating sudden soil weakening, possibly due to seismic activity or heavy rainfall causing groundwater rise. These landslides were likely triggered between 2009 and 2018 based on the dates of the aerial imagery. Identifying triggers for past landslides remains a major unresolved issue in landslide science. However, understanding these triggers is crucial for accurately assessing future landslide hazards.

Methodology In this paper, we investigate the possibility of earthquakes to precondition landslide development or reactivation during climatic events. By assuming a magnitude 5.2 earthquake, an epicenter of 10 km from this area, and different wetness conditions, the factor of safety (FS) and Newmark displacement (ND) models were calculated for shallow and deep-seated landslides with sliding depths of 3 and 7.5 m. Afterward, the relationship between FS, assumed ND, and observed landslides was analyzed in a cluster analysis, to derive patterns of climatically and seismically triggered landslides.

Results The comparison of FS maps and FS values of the observed landslides revealed that especially for landslides at 7.5 m depth, most sites that are stable during dry conditions become instable under saturated conditions, indicating a climatic trigger. At 3 m depth, however, some landslide sites that are still marginally stable under saturated conditions, display relatively high ND values for the investigated hypothetical earthquake, indicating a possible seismic influence. In the cluster analysis, we clustered the observed landslides according to their distances to rivers and topographic ridges and obtained three clusters. Landslides from cluster 3 with 31% of the landslides display medium to high ND for the assumed earthquake, and were found near ridges and farther away from rivers, suggesting seismic triggering. Cluster 2, with 12% of landslides closer to rivers, suggested climatic origins. Thus, while climate is a critical landslide contributing factor, seismic events may also contribute, either by predisposing to landslides or by reactivating them alongside climatic factors. These results enable the establishment of more precise and effective landslide mitigating measures considering mostly rainfall but also earthquakes as possible triggers.

Keywords Landslides, Earthquake, Newmark displacement, Soil geomechanical properties, Mount Oku, Cameroon volcanic line, Factor of safety

*Correspondence:
A. Braun
anika.braun@tu-berlin.de
Full list of author information is available at the end of the article

Introduction

The Cameroon Volcanic Line (CVL) represents a 1600 km long mega-shear zone and volcanic center in Central Africa (Déruelle 2007; Fitton 1980; Marzoli et al. 1999; Mfondoum et al. 2023; Moreau 1987; Ngapna et al. 2022). The CVL (Fig. 1) is associated with several natural hazards including volcanic eruptions, earthquakes, landslides, and toxic gas emissions from crater lakes (Bang et al. 2019). The largest earthquake with a magnitude of about 5.9 was recorded in 1945 near the contact between the Congo Craton and the Pan-African Belt at a depth of 10 km as mentioned by Ngatchou et al. (2018). Several earthquakes have been reported in Cameroon since the installation of the first permanent seismographic station in Yaoundé in February 1982 (Fig. 1c). Nnange et al. (1983) reported that this station recorded two earthquakes in 1983. The first with a local magnitude of Ml 3.9 occurred close to the northern margin of the Congo Craton at a locality called Tapare (East region), and the second with Ml 4.1 was located close to the Foumban shear zone in Magba (West region). Tabod (1992) and Nnange (2000) reported that one of the highest earthquake magnitudes of 4.8 was recorded in January 1987, close to the town of Tibati within the Foumban shear zone. It was felt at distances of over 250 km from the epicenter. In September 1983, an earthquake of magnitude 4.1 occurred near Magba and another one (Ml 4.6) near Monatele on March 19, 2005, at a depth of 11 km. The latter earthquake occurred within the seismic zone associated with the Foumbam Shear Zone (FSZ) and the northern margin of the Congo Craton (Cheunteu Fantah et al. 2022; Ndikum et al. 2014; Ngatchou et al. 2018).

The non-availability of monthly seismic data, landslide recordings, and monitoring systems in the CVL, restrains

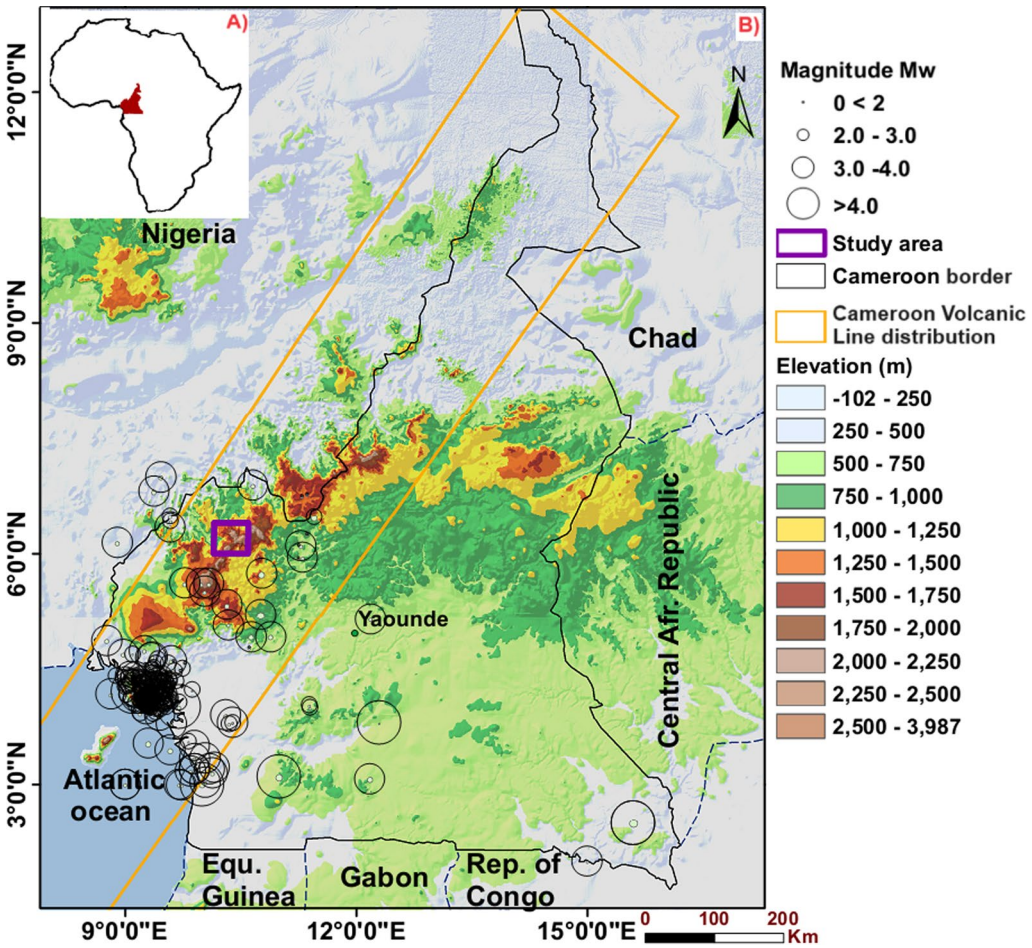

Fig. 1 Overview of the study area: **A** location of Cameroon within Africa (red irregular shape within the Africa map); **B** the study area (purple rectangle) in western Cameroon and a map showing the epicenters of earthquakes with homogenized moment magnitudes (Mw) recorded in Cameroon from 1909 to 2006 (compiled with data from Ambraseys and Adams 1986; Ateba et al. 1992; Ngongang et al. 2018; Ntepe et al. 2004; Tabod et al. 1992)

the evaluation of earthquake effects on landslide events in this seismically active region. Landslides along the CVL are commonly considered as being induced by rainfall by authors such as Ayonghe et al. (2004), Che et al. (2011), Wotchoko et al. (2016), and Djukem et al. (2020). However, few authors, such as Ayonghe et al. (1999) and Bang et al. (2019), affirmed that some landslides on the CVL have been induced by earthquakes. Ayonghe et al. (1999) reported that, on September 5th, 1995, a swarm of 57 landslides was triggered by an earthquake with an intensity of approximately IV on the Mercalli intensity scale at Bafaka, in the Southwest region of Cameroon. These earthquake-triggered landslides killed 3 people and destroyed farmlands and forests.

The landslide inventory mapped by Djukem et al. (2020), at the western flank of Mount Oku, revealed the presence of some landslides classified in this study as spreads or complex landslides from liquefaction. The study area includes approximately 20 villages with a population density of 162.3 people/km^2, based on the 2005 National Institute of Statistics census. This area is crucial for infrastructure, grazing, and agriculture in the northwest region (Djukem et al. 2020). In September 1997, July and September 1998, landslides in Belo caused a total of 9 deaths and damage to houses, farmland, and property (Ayonghe et al. 1999). These landslides suggest primarily the action of a sudden reduction of the shear strength which could be generated by seismic vibrations or rapid groundwater level increase due to rainfall. Understanding the specific triggers and mechanisms of these landslides will allow for more targeted and effective measures to reduce landslide risk and protect lives and property in vulnerable areas in this region.

Rainfall and earthquake-induced landslides differ in terms of mechanics and dynamics, as reported by Crozier (2005) and Chang et al. (2007). Earthquake-induced landslides tend to be more massive and occur in clusters near ridges (Rana et al. 2021, 2022). Discriminating between rainfall and earthquakes as possible triggers of past landslides is still an unresolved question in landslide science and paleoseismology. Some recent approaches include using the geometry of landslide bodies to classify observed landslides into rainfall- and earthquake-triggered using statistical methods (Qiu et al. Qiu et al. 2024; Rana et al. 2021, 2022), or using numerical modeling to back-analyze observed landslides (Mreyen et al. 2022). Here, we propose to combine a deterministic geotechnical approach based on the Newmark displacement (ND) method (Newmark 1965) for assessing the slope performance under seismic shaking with a statistical analysis of observed landslides and a cluster analysis. Originally developed for dams, in the ND method the slope is abstracted as a rigid block on an inclined plane and the accumulated displacement of this block whenever a critical acceleration threshold is exceeded during an earthquake is quantified (Jibson et al. 2000). The ND is linked to the static factor of safety (FS), which allows assessing the static equilibrium of a slope based on geotechnical soil properties and water saturation for an assumed depth of the sliding surface. In 2000, Jibson et al. proposed a simplified framework for computing the ND in a geographic information system (GIS) based on an empirical relationship they established between some earthquake records and induced landslides. In 2007, Jibson published further empirical equations for assessing the ND, based on a larger body of data.

The cluster analysis (Alkarkhi and Alqaraghuli 2020; Venkatramanan et al. 2019; Zhang et al. 2023), is a multivariate statistical analysis method, which allows through an unsupervised learning approach to group data into a given number of clusters. The cluster analysis has been used in many fields, e.g. for the investigation of water quality (Alkarkhi and Alqaraghuli, 2020), classification and evaluation of reservoirs (Zhang et al. 2023), and analysis of the spatial heterogeneity of physicochemical parameters (Venkatramanan et al. 2019).

In this study, we investigate the possibility of small seismic events to precondition landslide development or reactivation during climatic events at the western flank of Mount Oku. To determine whether climate- and earthquake-induced landslide patterns exist, we combine deterministic methods commonly used in geotechnical engineering practice and statistical approaches. First, deterministic approaches including the FS and ND will be implemented. The FS will allow evaluating the failure conditions of these slopes by assuming shallow and deep-seated landslides with sliding depths of 3 and 7.5 m; and different slope saturation levels to account for possible rainfall triggering (Doglioni et al. 2013; Johari and Javadi 2012; Keles and Nefeslioglu 2021; Okimura and Kawatani 1986). Additionally, we will assess the stability of these slopes under given seismic shaking conditions using the ND method (Djukem et al. 2024; Jibson 2007; Newmark 1965; Yuan et al. 2016), which also reflects the potential effects of a future earthquake occurring close to the study area. Second, the cluster analysis will allow the quantitative evaluation of earthquake- or rainfall-induced landslide patterns among the landslides inventoried.

The study area

Relief

This investigation was carried out on a study site of approximately 1000 km^2. This area is located around latitude 6° 2′ 20″ N to 6° 25′ 23″ N and longitude 10° 11′ 39″ E to 10° 35′ 46″ E on the western flank of Mount Oku.

The western flank of Mount Oku presents a humid, tropical, highland climate with two seasons. The rainy season extends for eight months (April to November). The dry season extends for four months (December–March). The total annual precipitation is 2546.5 mm, with a maximum of 579.6 mm observed in July and a minimum of zero in December. The average annual rainfall data used in this study comes from the "Northwest Regional Service for Meteorology" in Bamenda, Cameroon. This data was recorded between 2005 and 2010, as cited by Djukem et al. (2020).

The western flank of Mount Oku is characterized by highly variable topography, which reflects the past geological and erosional processes. Hillsides have very steep slopes and valleys present convex "V" or "U" shapes, as can be observed on topographic profiles (Fig. 2). Interfluves are peaked, rounded (western border of the Ndop plain) or flat (around Kumbo). The landscape includes steep hill slopes (talus and escarpments), deeply incised valleys, undulated and flat landscapes. The elevation ranges from 100 m in plains to about 3000 m around Mount Oku summit. This zone is made up of mountain peaks whose altitudes vary between approximately 1100–3000 m as shown by the map in Fig. 2. The northern flank of Mount Oku shows valleys and variable interfluves in staircase steps towards Lake Nyos. The eastern flank presents an escarpment in the direction of the Ndop plain. The western flank of Mount Oku presents very gentle slopes (0–15°) and gentle slopes (15–25°) occupy the largest surface of this area (74%), while steep slopes ranging from 24–31° and very steep slopes > 31° occupy 24% of the total surface (Fig. 3).

Geological setting

Mount Oku is in the western part of the Cameroon Volcanic Line (CVL), characterized by an alignment of oceanic and continental volcanic massifs, and plutonic complexes as presented by Marzoli et al. (1999); Déruelle et al. (2007); Kamgang et al. (2007); Kamgang et al. (2010) and Gountié et al. (2011). The Oku volcanic group (OVG) is a complex stratovolcano of approximately 90 km in diameter and 3011 m height more specifically found at the central part of the CVL continental sector (Njilah et al. 2007). This OVG shelters four major stratovolcanoes which are: Mount Oku, Mount Babanki, Nyos and Nkambe (Woolley 2001), as presented by Marzoli et al. (1999); Déruelle et al. (2007); Kamgang et al. (2007); Kamgang et al. (2010) and Gountié et al. (2011). The study area is covered by highly weathered basalt with thick residual soil, slightly weathered rhyolite with no residual soil, moderately weathered trachy-rhyolite with very steep slopes, and highly weathered migmatites with moderately steep slopes. Trachy-rhyolite and basalt are the dominant rock types in the study area, with area percentages of 37% and 54%, respectively.

The geomechanical properties of the soils developed on these rocks are presented in Table 1 and Fig. 4. These soils originate from the physical and chemical weathering of these bedrocks either in place, or during their transportation over long distances, after which they are deposited in lowlands. They are mostly clayey soils with high to very high plasticity and swelling capacities (Djukem et al. 2020).

Materials and methods

Investigated landslides at the western flank of Mount Oku—widespread shallow or complex slides

The landslides investigated in this work consist of 179 small- to large-size, shallow to deep slides, debris flows, and complex slides from liquefaction or flow processes that were previously presented by Djukem et al. (2020). They were recorded and mapped with the use of the MapSource application (Garmin Ltd., Schaffhausen, Switzerland), Google Earth (Google LLC, Mountain View, California, USA), and ArcGIS software (ESRI Inc., Redlands, California, USA). These landslides are also used in the present study to validate the physical landslide models. The prediction landslides include 75% of the landslides (42,147 pixels) and the validation landslides include 25% (14,067 pixels) of the total landslide pixels. The validation landslides are the most recent ones (see Djukem et al. 2020). Some of these recent landslides include some spreads or complex slides that seem to be from liquefaction (area encompassed by the orange circle in Fig. 5). They are visible in the Google Earth aerial images of 2018, but not in the images of 2009 (based on the Google Earth aerial imagery's dates in Fig. 5C and D. However, Fig. 5D corresponds to the 2021 aerial image, which is clearer than the 2018 one). As already investigated by Djukem et al. (2020), eleven representative soil samples were taken on failure and non-failure sites, from soils developed on each rock type, flat and sloping areas, in forested and non-forested areas, and close to major rivers and roads, at depths varying between 0.25 and 7.3 m. These soils included disturbed and undisturbed samples from which particle density, bulk density, moisture content, friction angle, and cohesion were determined among others.

Static factor of safety calculation with the infinite slope model (ISM)

Deterministic models of slope stability such as the FS require detailed laboratory derived soil parameters and field measurements. These models provide the best quantitative information on landslide susceptibility

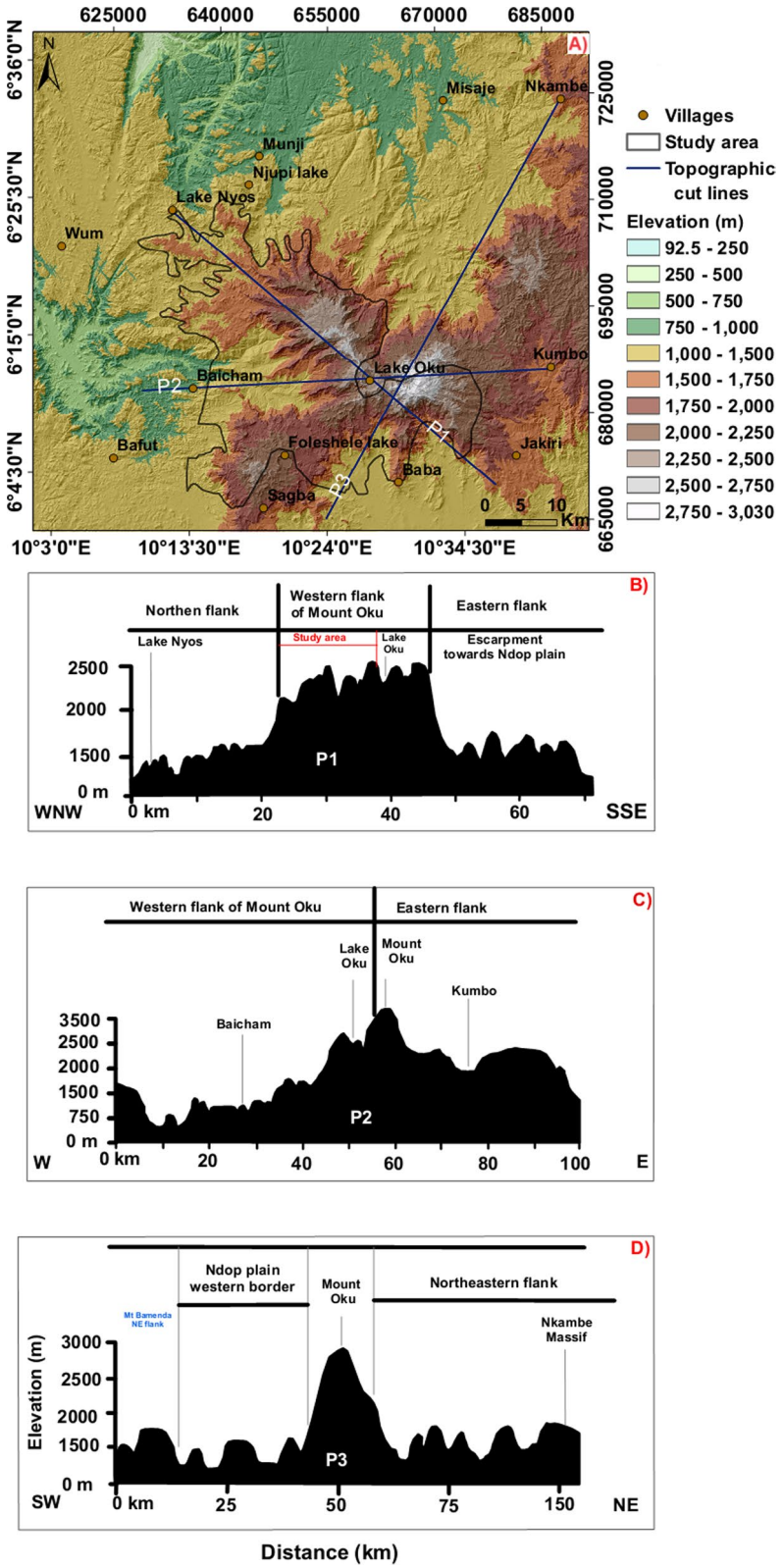

Fig. 2 Relief of the Mount Oku shown by TanDEM-X digital elevation model showing variations in terrain elevation, with outline of the study area by the black polygon (**A**). Schematic topographic cross-section through Mount Oku and surrounding zones: WNW-SSE (**B**), W-E (**C**), and SW-NE (**D**) sections. Please note the different horizontal scales

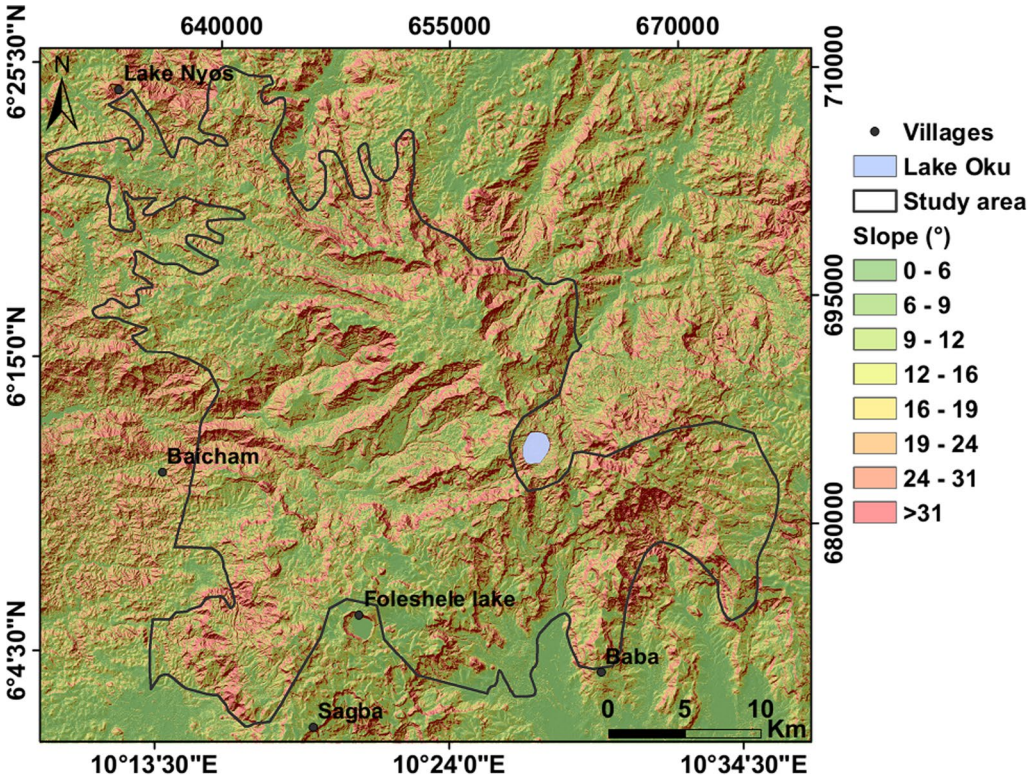

Fig. 3 Morphology of the western flank of Mount Oku with the study area highlighted by the dark polygon

Table 1 Soil geomechanical properties: cohesion, internal friction angle, wetness, bulk density, and particle density

Soil properties	Soil on basalt	Soil on trachy-rhyolite	Soil on migmatite	Rhyolite outcrop
Particle density (g/cm^3)	26.66	25.99	29	25
Bulk density (g/cm^3)	15.01	14.59	15.84	0
Moisture content (%)	41.2	44.1	39.3	0
Friction angle (°)	23.6	16.8	31.5	46
Cohesion (kPa)	25.4	33.2	47.7	13,000

(Doglioni et al. 2013; Keles and Nefeslioglu 2021; Okimura and Kawatani 1986; Van Westen 2004). The best fitting FS scenarios are expected to capture more landslides in the instable and marginally stable FS classes, with $FS < 1$ and $1 \leq FS < 2$, respectively. These classes correspond to the most susceptible.

The ISM is based on the assumptions that the slope is uniform, homogeneous, and unlimited. The failure surface and groundwater table are assumed to be parallel to the ground surface. The failure block is considered infinitely long and wide so that stresses are the same on the two planes perpendicular to the slope. The ISM is used to calculate the FS, using the mathematical formula below:

$$FS = \frac{c}{\gamma \cdot t \cdot \sin\alpha} + \frac{\tan\phi}{\tan\alpha} - \frac{m \cdot \gamma_w \cdot \tan\phi}{\gamma \cdot \tan\alpha} \quad (1)$$

where c is the cohesion (kPa), ϕ the internal friction angle (rad), α the slope angle (rad), t the total layer thickness or depth of slip surface (m), γ the material unit weight (kN/m^3), γ_w is the unit weight of water (kN/m^3), and m is the thickness of the saturated layer. For fully saturated conditions ($m = 1$) the phreatic surface is at the ground surface. In dry conditions ($m = 0$), the phreatic surface is

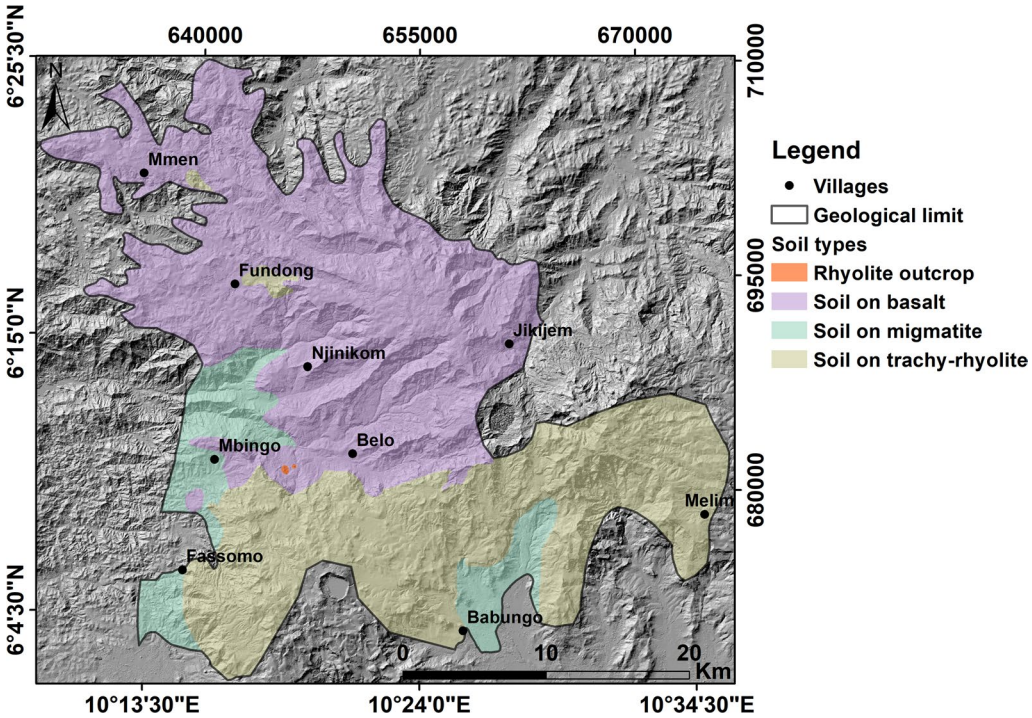

Fig. 4 Soil types of the western flank of Mount Oku (the geological limit is highlighted by the dark polygon)

below the failure plane and does not affect the stability. The natural moisture conditions obtained in the laboratory is m = w.

To investigate the combined seismic and climatic influence on the destabilization of Mt. Oku's slopes, we consider different scenarios of landslide depths and water saturation. The thickness of the potential sliding layer value "t" was varied between 3 and 7.5 m (representing the maximum failure depth observed in the study area). The water saturation varies between dry conditions (m = 0), natural moisture conditions (m = soil moisture content measured in the laboratory), and fully saturated conditions (m = 1).

Seismic slope stability calculation with Newmark displacement method

The ND method simulates seismically induced slope behavior, specifically the displacement, considering the latter as a rigid block on an inclined plane (Jibson et al. 1998; Jibson et al. 2000; Jibson 2007; Kumar et al. 2021; Miles and Ho 1999; Newmark 1965). The method provides information on the slope performance in the form of permanent displacement (Havenith et al. 2006; Kumar et al. 2021; Miles and Ho 1999). The ND is derived from an acceleration time history by integrating twice the values larger than the critical acceleration (a_c) required to induce sliding. Mathematically, it is calculated in this work according to Eq. (2) by Jibson (2007).

$$\log(D) = 2.401.\log(Ia) - 3.481 \cdot \log a_c - 3.230 \pm 0.656 \quad (2)$$

where Ia is the Arias intensity, and a_c is the threshold acceleration required to initiate sliding in terms of the acceleration of the Earth's gravity, g.

Ia can be considered as a quantitative measure of the degree of shaking of an earthquake. It can be calculated following Eq. (3), proposed by Keefer and Wilson (1989), valid for earthquake moment magnitudes Mw below 7.

$$\log I_a = -4.1 + M - 2\log R + 0.5P \quad (3)$$

where M is the earthquake magnitude ($M_w = 5.2$ assumed in this case, since earthquakes recorded in this region within the last one hundred years are of local magnitude Ml below 5), R the hypocentral distance (here 10 km since the closest earthquakes to the study area are located at a distance of about 80–200 km) at depth of 10 km, I_a of 0.41 ms calculated with Eq. (3) and P is a probability term including possible variations and uncertainty, here assumed to be 0. These equations are in fact empirical equations correlated with several worldwide earthquakes data by these authors.

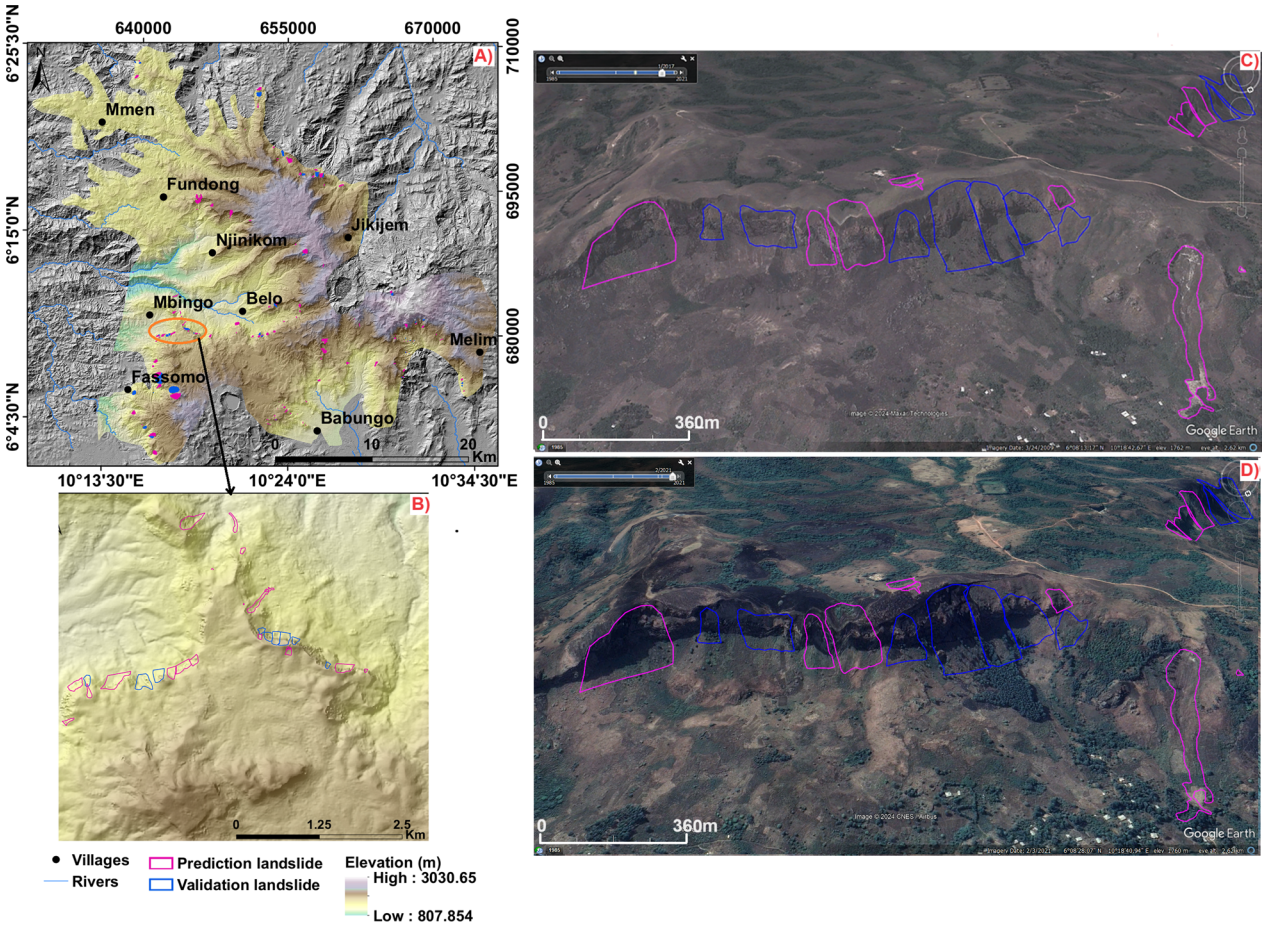

Fig. 5 Spatial distribution of landslides recorded between 2009 and 2018; the blue and pink polygons represent prediction and validation landslides (**A** and **B**); **C** and **D** show the Google Earth aerial images of 2009 and 2018, highlighting areas affected by spreads or complex landslides. The March 24, 2009, image **C** has been provided by Google Earth, © 2024 Maxar Technologies. The February 3, 2021, image **D** has been provided by Google Earth, © 2024 Airbus

The critical acceleration a_c is linked to the factor of safety FS resulting from the infinite slope model, and to the slope angle by means of g (9.81 m/s^2), calculated by means of Newmark (1965); Jibson et al. (1998); and Miles and Ho (1999); Jibson (2007) equations.

$$a_c = (FS - 1) \cdot g \cdot \sin\alpha \tag{4}$$

where a_c is the critical acceleration in m/s^2, FS is the factor of safety, g is the acceleration due to gravity (9.81 m/s^2), and α is the slope angle in rad.

The process for calculating ND, as described above, is summarized in Fig. 6.

Computation of FS and ND maps

The six FS and corresponding ND scenarios were computed in ArcGIS 10.5 following the steps below.

In step 1, the slope angle map was derived from the 12 × 12 m cell size TerraSAR-X add-on for Digital Elevation Measurements (TanDEM-X DEM) standard product 0.4 arcseconds with 12.37 m resolution at the equator kindly provided for this research by the German Aerospace Center (DLR), see Djukem et al. (2020).

In step 2, the geological map was prepared using existing maps as explained by Djukem et al. (2020). Soil cohesion, internal friction angle, wetness, and unit weight mean values were taken from the laboratory test results of Djukem et al. (2020), attributed to the corresponding geological units, and converted into raster files.

In step 3, the different FS and ND scenarios as described above were computed with the raster calculator tool of the ArcGIS 10.5 Spatial Analyst tools based on Eqs. (1), (4), and (2).

It should be noted that the TanDEM-X has been recorded between 2011 and 2015. Thus, it reflects the

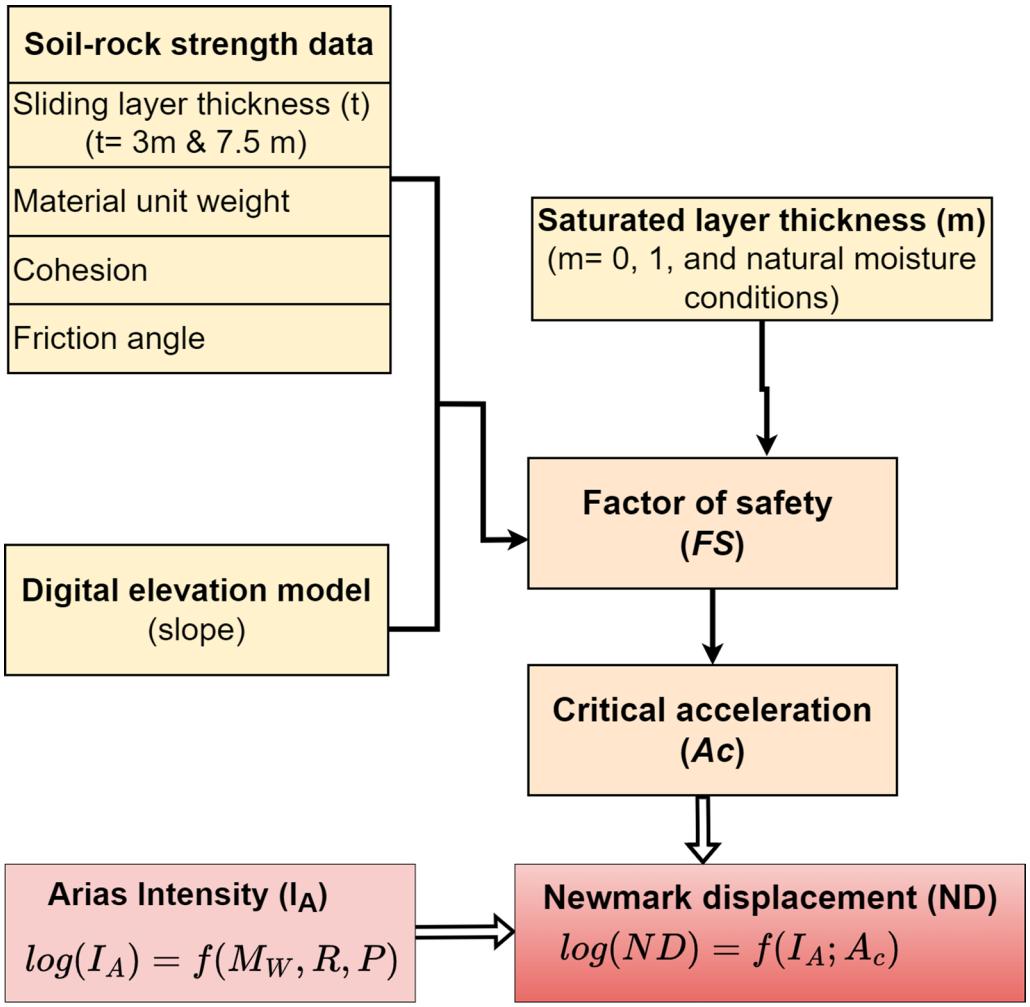

Fig. 6 The Newmark displacement (ND) calculation flow chart

post-failure topography for the prediction landslides mapped from the 2009 Google Earth images, and the pre-failure topography of the validation landslides that were mapped based on the 2018 Google Earth images.

Analysis of FS and ND values of observed landslides

We quantify the relationship between FS, ND, and observed landslides through the examination of FS and ND values within each observed landslide. For this purpose, we used the tool "Zonal statistics" in QGIS to extract the min, max, and mean values of all FS and ND scenarios for each landslide polygon (179 polygons).

Identification of landslide clusters

To investigate whether patterns of climatically and seismically triggered landslides could be identified, a cluster analysis was performed based on different topographic parameters of the observed landslides. Seismically and climatically induced landslides can be characterized by specific geometric and topographic patterns (e.g. Qiu et al. 2024; Rana et al. 2021, 2022). For instance, seismically induced landslides tend to occur at mountain tops or ridges with smaller slope angles, while climatically induced landslides tend to occur around the slope foot, close to rivers, and at steeper slope angles. We systematically examined the morphological properties of landslides in the Mount Oku area with a k-means cluster analysis in IBM SPSS Modeler to identify possible clusters of landslides.

In step 1, we generated a dataset of different morphological properties that were all based on the 12.5 m resolution TanDEM-X DEM. The parameters are distance to ridges (minimum over landslide polygon), distance to rivers (minimum over landslide polygon), slope angle (maximum within polygon), slope aspect, and curvature (both mean within landslide polygon). The distance to ridges was generated by firstly deriving the landform "ridges" using the TPI-based landform

classification tool in QGIS/SAGA with the radiuses of 300 m and 1200 m and secondly computing the proximity with the proximity tool in QGIS. The distance to rivers was computed using the proximity tool with the river network extracted from the DEM. Slope angle, slope aspect, and curvature were generated in QGIS/SAGA with the "Slope, Aspect, Curvature" tool. Then, for each landslide body the minimum, maximum, or mean, respectively, of these parameters were extracted using the "Zonal statistics" tool in QGIS.

In step 2, k-means cluster analysis was performed in IBM SPSS Modeler, for different combinations of two and three parameters and different numbers of clusters (between one and seven) for each combination. In each run, in an iterative process, the first cluster center is assigned according to the values of the first record in the dataset. For each record, the distance to the first cluster center is calculated and a second cluster center is set to the record with the largest distance to the first center, and so on, until the defined number of clusters k is achieved. Now, each data point is grouped to the cluster center with the smallest distance. Then, the locations of the cluster centers are moved to the average of each cluster, and this process is reiterated until the maximum number of iterations is reached or there is no change in the cluster centers anymore (Wendler & Gröttrup 2021). The process is repeated for different numbers of clusters k and the sum of the squared distances of each point to its closest cluster centroid is plotted against the number of clusters (elbow plot) to determine the optimal number of clusters. In the elbow plot, see Fig. A2 in the Appendix/Supplementary material, the sum of squared distances usually declines with increasing number of clusters k, and at a certain point, there is an "elbow" in this trend, where the increase of the number of clusters only results in a slight decline of the sum of squared distances. This point is considered to indicate the optimal number of clusters.

It should be noted that the k-means clustering is sensitive to the initial placement of the cluster centers. In the IBM SPSS Modeler, this depends on the order of the data. To exclude any effects of the data order on the resulting clusters, we tried different ways to order the data. The baseline case is ordered by landslide ID, moreover, we ordered the data ascending or descending by distance to ridges and distance to rivers, respectively.

Results and discussion

To explore possible patterns of climatically or seismically induced landslides, we first present, discuss, and interpret the spatial distribution of FS and ND values, then the relationships between FS, ND, and the observed landslides, and finally we analyze the relationship between topographic factors of the observed landslides through the k-means clustering analysis.

Infinite slope model-based factor of safety

Factor of safety for shallow landslides with depth of failure t = 3m

Six FS maps have been computed according to Eq. (1) for landslides at two different depths (3 m and 7.5 m) and with different water saturation levels (dry conditions, natural moisture conditions, saturated conditions). The FS maps have been classified into four slope stability degrees: $FS < 1$ denotes instable slopes, $1 \leq FS < 1.5$ slopes at the point of failure, $1.5 \leq FS < 2$ represents critical stability slopes and $FS \geq 2$ indicates stable conditions.

The scenarios assuming shallow landslides at 3 m depth display FS values between 0.61 to $FS \geq 2$ (Fig. 7a, b, and c). The proportions of the four stability classes increase from dry (yellow bar) to full saturation (dark blue bar) conditions. These shallow landslide scenarios display almost no instable areas with $FS < 1$ (about 2% of the total surface). The percentage of the stable domains with $FS \geq 2$ is dominant in all the saturation conditions (from 72 to 86%). The proportions of slopes at the point of failure ($1 \leq FS < 1.5$) vary between 4 and 11%. The proportions of critical slopes ($1.5 \leq FS \leq 2$) fluctuate between 10 and 14% (Fig. 7d).

Factor of safety for deep landslides with depth of failure t = 7.5m

The scenarios assuming deep landslides at 7.5 m depth display lower FS values, that vary between 0.26 and 8 120 (Fig. 9a, b, and c). Similar to the shallow landslide scenarios, the percentage of the stable domains with $FS \geq 2$ (33–60% of the total surface), is greater than the proportion of the instable areas with $FS < 1$ (8–28%), in all saturation conditions (Fig. 8d). The variation of the proportions of the four stability classes also increases from dry (yellow bar) to full saturation (dark blue bar), in 75% of the saturation conditions. The proportions of slopes at the point of failure vary between 17 and 24%. The proportions of critical slopes fluctuate between 15 and 17% (Fig. 8d). The scenario assuming deep landslides of 7.5 m depth, shows all the classes of stability: instable, at the point of failure, critical, and stable. This scenario seems to be a better representation of the real situation observed in the western part of Mount Oku, where landslides and non-landslide areas are observed.

Considering the saturation conditions, the disparity observed between the stability classes highlights the influence of the groundwater level on slope

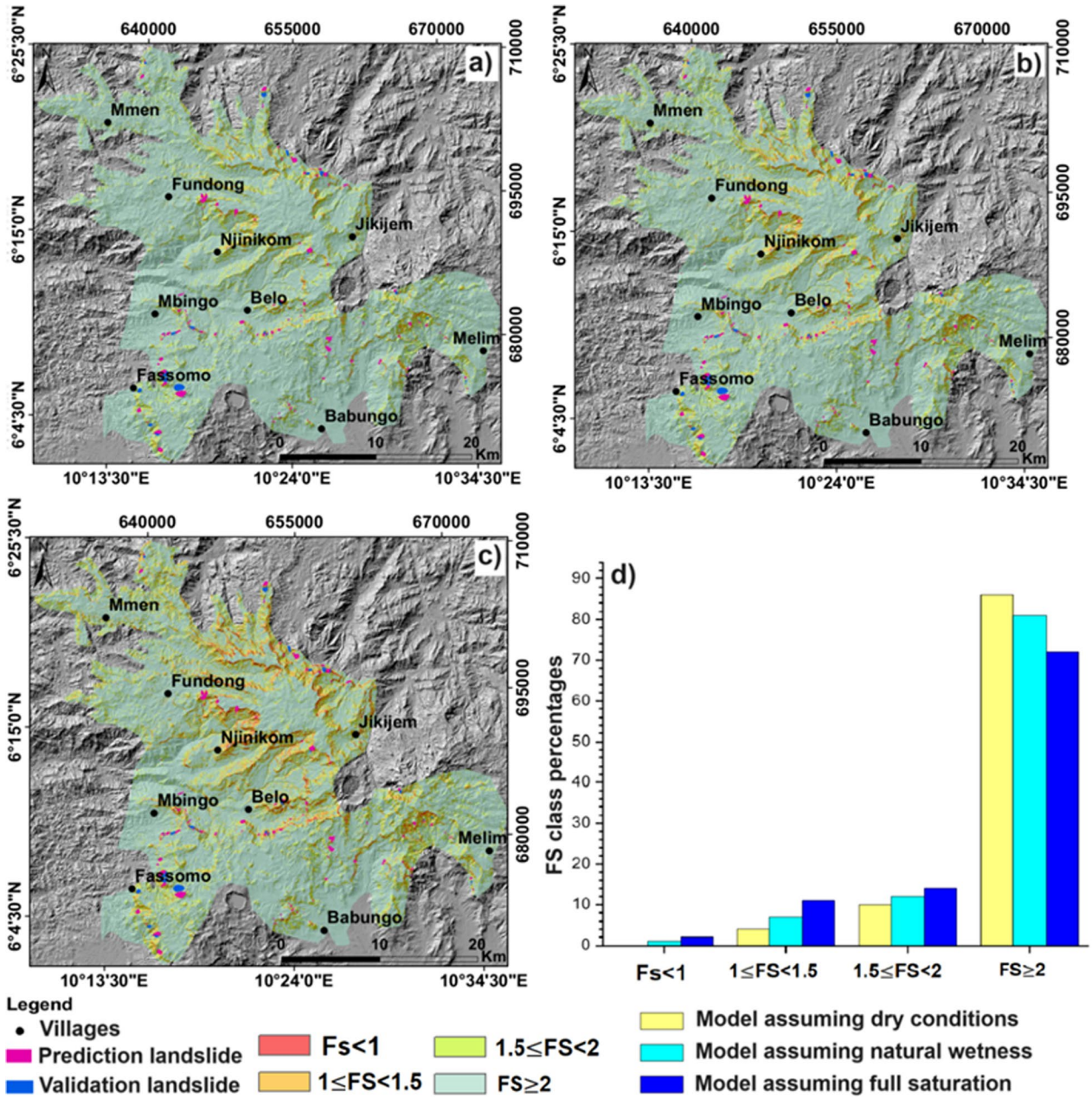

Fig. 7 Factor of safety at 3 m depth, in dry conditions (**a**), natural wetness conditions (**b**), dry conditions (**c**); and stability class percentages (**d**)

stability. Moreover, landslide depth, soil cohesion, friction angle, and shear stress affect the shear strength and the stability of a soil mass against potential failures as shown by Miles and Ho (1999). The increase of the groundwater table due to rainfall increases the probability of landslide occurrence, as also confirmed by Alsubal et al. (2018) in their study on the rise of groundwater due to rainfall and the control of landslides by zero energy groundwater withdrawal system. These FS scenarios assuming shallow and deep landslides can therefore be used as an efficient predictive tool for future shallow and deep landslides even in case of extreme climatic conditions.

Newmark displacement

According to the six FS scenarios at two different depths and at three different saturation levels, six different ND maps were computed based on Eqs. (4), (2) and Fig. 6 for the scenario of an Mw = 5.2 earthquake in 10 km

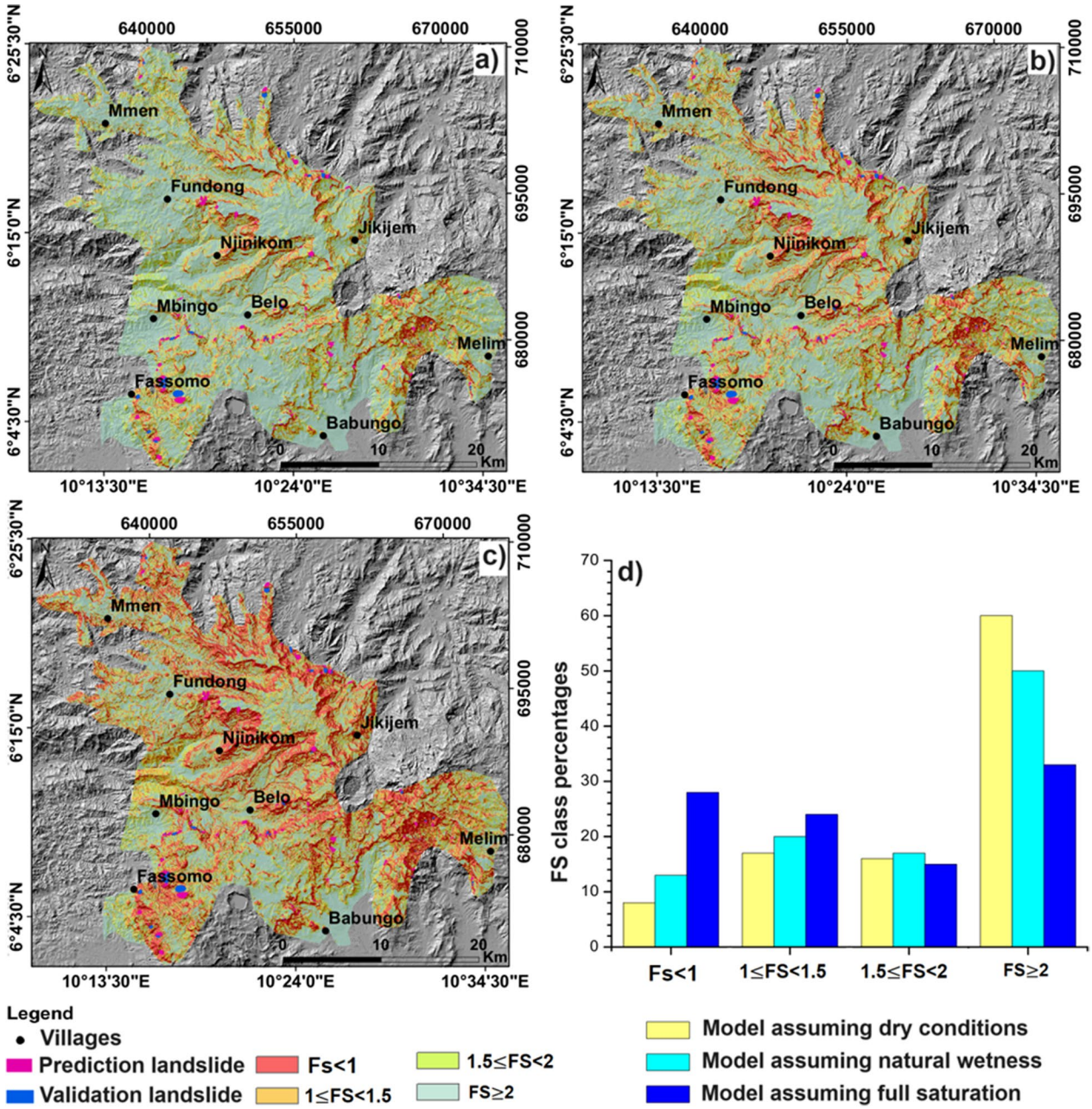

Fig. 8 Factor of safety at 7.5 m depth, in dry conditions (**a**), natural wetness conditions (**b**), dry conditions (**c**); and stability class percentages (**d**)

epicentral distance. The maps in Fig. 9 show the resulting ND for landslides with an assumed sliding surface at 3 m depth (a and b) and 7.5 m depth (c and d), at dry conditions (a and c) and fully saturated conditions (b and d). The maps show that areas with higher ND values follow the areas with low FS values and steep slopes, whereas the areas with soil on migmatite in general show lower ND values than the areas with soils on basalt and trachy-rhyolite.

These ND values represent the failure probability of these slopes under seismic stress (Jibson 2007; Djukem et al. 2024). Additionally, the interpretation of these values varies between plastic soils and rigid brittle rock materials. In the Mount Oku area, the soils are deep and clayey. Thus, it could be assumed that larger ND values are required to indicate the seismic triggering of a

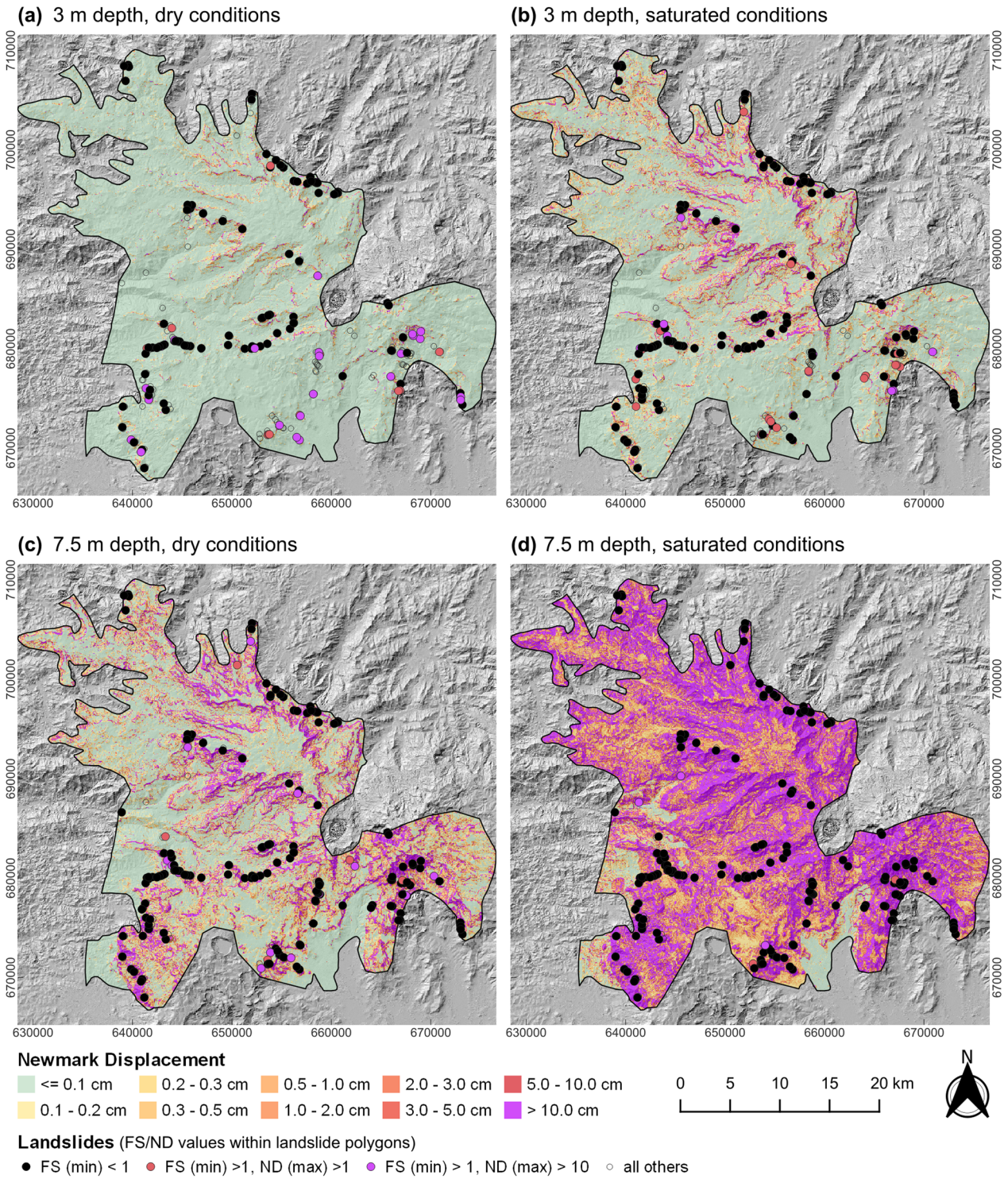

Fig. 9 Newmark displacement and locations of the min within polygon for shallow and deep landslides: **a** 3 m depth and dry, **b** 3 m depth and saturated conditions, **c** 7.5 m depth and dry, and **d** 7.5 m depth and saturated conditions

slope failure. In Fig. 9, especially under saturated conditions and for deeper sliding surfaces, higher ND values beyond 10 cm (purple colour in the maps) are reached widely, going beyond the areas that already have a critical FS (compare Fig. 9 with Figs. 7 and 8). This indicates on the one hand a potential for seismic triggering of deeper landslides in the study area. On the other hand, it also indicates the potential for seismic acceleration to push

slopes that already have a marginally stable FS value under saturated conditions into failure. In the next section, this will be investigated in more detail for the landslides observed in the study area.

Analysis of FS and ND values of the observed landslides

In this section, we investigate how well the calculated FS and ND scenarios can explain the landslides observed in the Mount Oku area. We also discuss the implications of these findings for identifying the primary triggering factor of these landslides.

FS values of the observed landslides

Landslides with FS greater than 1 (thus stable) but having a high ND value, could indicate a seismic trigger for these cases. Landslides with FS greater than 1 that become instable under saturated conditions, would point rather at a climatic trigger.

For the sake of simplicity, here we grouped the slopes at the point of failure ($1 \leq FS < 1.5$) and critical stability slopes ($1.5 \leq FS \leq 2$) under the appellation marginally stable slopes ($1 \leq FS \leq 2$). In Fig. 10, we plotted the percentage of landslides that fall into each of these three categories considering the minimum FS value within each landslide polygon for the FS scenarios at the two different depths and three different moisture conditions. Please note that we differentiated between prediction and validation landslides here, as the FS was based on a DEM that was created after the prediction landslides occurred and before the validation landslide occurred. Thus, the DEM represents post-failure conditions for the prediction landslides and pre-failure conditions for the validation landslides, which could have implications for the following interpretations.

The FS scenarios with good landslide predictive ability should show a decreasing trend, having the greatest number of landslides in the first lowest FS classes ($FS < 1$ and $1 \leq FS \leq 2$), corresponding to the most susceptible classes. This trend can in general be observed for all FS scenarios in Fig. 10, and as can be expected, it is more pronounced

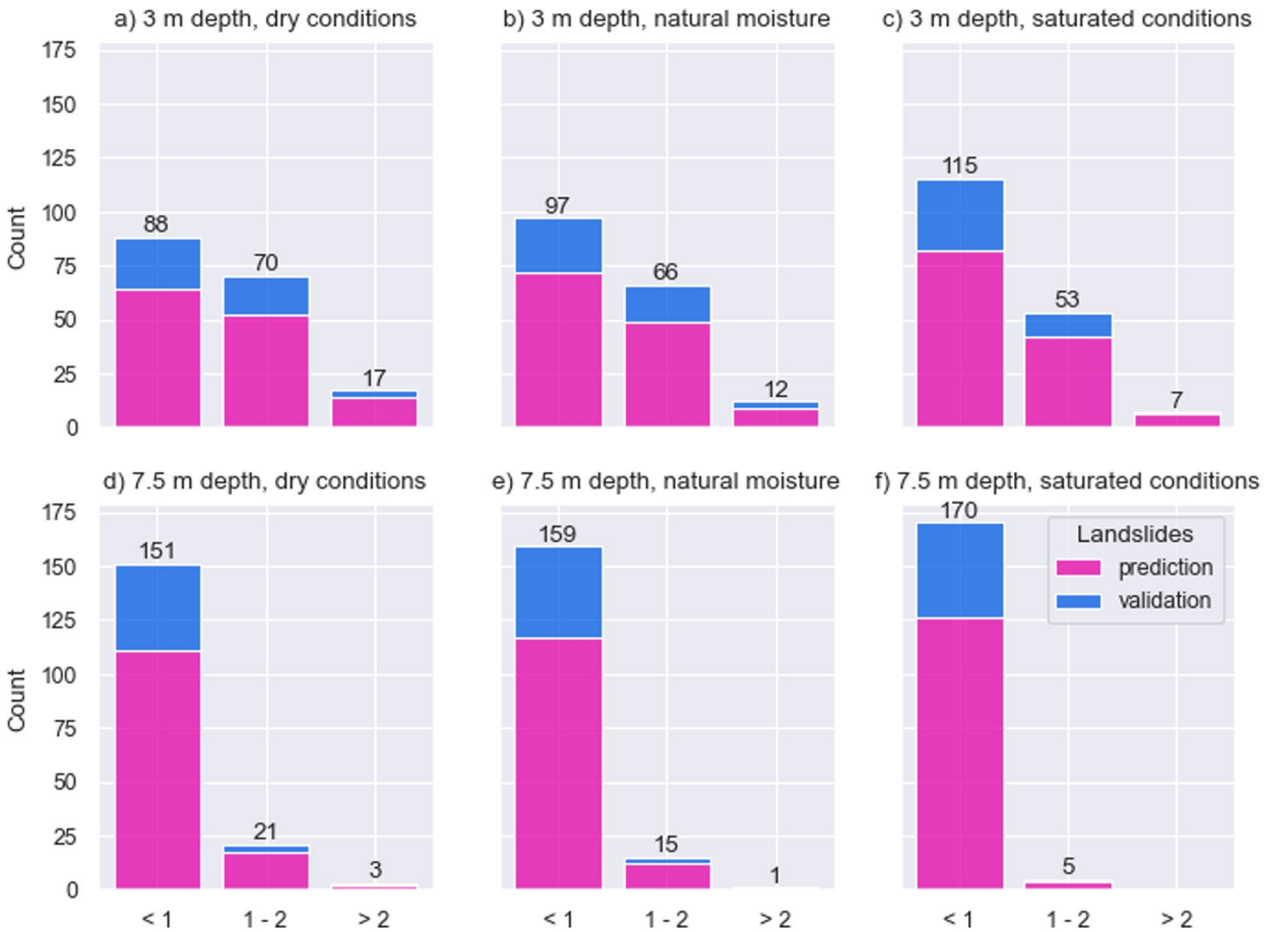

Fig. 10 Distribution of the factor of safety values at 3 m (**a**, **b**, **c**) and 7.5 m depth (**d**, **e**, **f**) within the instable (< 1), marginally stable (1–2), and stable (> 2) domains as minimum value within polygons of observed landslides

for the saturated scenarios and the scenarios at the greater depth. With the percentage of the first bar in the instable domain (FS < 1) corresponding to the true positive rate of the respective FS scenarios, it can be observed that at an assumed depth of the sliding surface of 3 m 50% of the observed landslides can be captured under dry conditions, 90% considering also the marginally stable cases, while this number increases to 65% under saturated conditions or 95% considering the marginally stable cases. In all three scenarios at 3 m depth, some observed landslide cases cannot be explained by the FS alone as they fall into the stable domain.

At an assumed depth of the sliding surface of 7.5 m, the picture looks different. Over 86% of the observed landslides fall into the instable domain under dry conditions, and 97% under saturated conditions, with only very few to zero cases under the stable domain in all three scenarios.

Regarding the pre- versus post-DEM landslides, it could be expected that particularly the post-DEM landslide locations would represent instable conditions, as a failure did occur there shortly after the DEM was created, while for the pre-DEM landslides the slopes might have reached a stable state in terms of slope angle, which would lead to stable FS values for these cases. Only very few post-DEM landslide cases fall into the stable domain (Fig. 10). Moreover, the presence of pre-DEM landslides in the stable domain could be explained as above, by the fact that after failure the slope has transitioned into an equilibrium and stable state. Thus, these cases would not necessarily count as missed predictions.

To draw some conclusions on the role of rainfall as a trigger of the landslides at Mount Oku, we can see that at a depth of 3 m, the presence of water in the slopes does push the percentage of landslide in the instable domains from 50% at dry conditions to 55% at natural moisture conditions and 65% under full saturation. For the landslide cases in the marginally stable and stable domains, an additional triggering factor, such as an earthquake, could be considered, as will be discussed in the following Sect. "Combined analysis of FS and ND values of observed landslides".

At the depth of 7.5 m the same trend can be observed, but it is less pronounced. The percentage of landslides in the instable domain increases from 86% under dry conditions to 90% under natural moisture conditions and 97% under saturated conditions. Thus, for landslides at 7.5 m depth, rainfall would be a sufficient explanation as triggering factor.

Combined analysis of FS and ND values of observed landslides

As discussed above, landslide cases that fall into the marginally stable or stable domain of the different FS scenarios might have to be explained by additional triggering factors, such as earthquakes. These cases were highlighted in the maps in Fig. 9 Here, black circles indicate landslide sites with stable FS and low ND. Filled black dots indicate instable landslide locations with an FS < 1. Red dots indicate landslide locations with FS > 1 (stable) and ND > 1. Purple dots indicate stable landslide locations with FS > 1 and very high ND > 10. Under the assumption that a slope movement is usually initiated when ND > 1 (Bray 2007; Delgado et al. 2020), or when ND > 10 for the deep clayey soils in the study area, purple dots could indicate potentially earthquake-induced landslides for the scenario of an earthquake of Ml = 5.2 that was assumed for these simulations.

These maps allowed determining which landslides are found in stable areas under dry conditions, but instable under saturated conditions, suggesting rainfall as trigger. Also, we identified landslide locations with FS > 1 and very high ND > 10 suggesting potentially earthquake-induced landslides. For the shallow landslide scenario at 3 m depth, there are quite a few landslides that fall into this category, especially under dry conditions, but also under saturated conditions. To investigate this further, we created a Sankey diagram that shows the transition of landslide locations from dry to saturated conditions, and the ND at dry conditions (Fig. 11). Part of the marginally stable sites during dry conditions transition to instable conditions during full saturation of the slope. Only very few cases of slopes that remain stable during full saturation have a medium ND, indicating a possible seismic trigger.

It becomes apparent that there are some landslides with an FS > 1 and quite high ND values, but most of them have an FS < 2, thus, they were marginally stable anyway. This suggests that these slopes were already marginally stable, and an earthquake could push them over the edge to instability, but so could a rainfall event. It should be kept in mind that the ND values were computed for a hypothetical Ml = 5.2 earthquake at 10 km distance. Due to the lack of local earthquake records, we do not know whether a similar earthquake happened in the past. However, according to other earthquake records in the region, it is not unrealistic.

For the deeper scenario of landslides with an assumed sliding surface at 7.5 m depth there are only very few cases that are in the marginally stable FS domain. They are not further discussed here, as the FS alone already explains these deeper landslides sufficiently.

K-means cluster analysis of the results

Distance to ridges and rivers seem to be important characteristics of seismically/climatically induced landslides as also suggested by Rana et al. (2021), Rana et al.

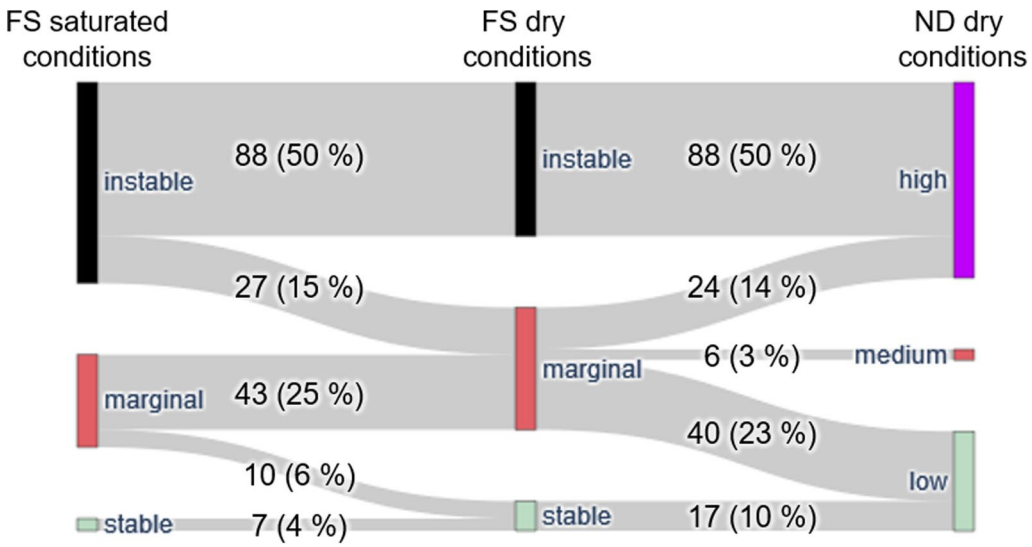

Fig. 11 Transition of factor of safety (FS) state (instable: FS < 1, marginally stable: 1 < FS < 2, stable: FS > 2) of landslides at 3 m depth from dry to saturated conditions (middle to left) and to high (> 10), medium (2–10) and low (< 2) Newmark displacement (ND) in the dry case during an earthquake (middle to right), with min FS and max ND within polygons

(2022), and Qiu et al. (2024). We explore the relationship between landslide distance to ridges and rivers using a k-means cluster analysis. We also explored slope angle, slope aspect, and curvature in the analysis. However, in the following, we will focus on distance to ridges and distance to rivers as this combination resulted in the lowest sums of squared distances and is easier to interpret. Moreover, we explored the effect of data ordering on the resulting clusters, as the analysis is sensitive to the initial placement of the clusters which is in our case depending on the data order. In four out of five different ways to order the data, we yielded the same clusters, which we thus considered the most robust. More information can be found in the Appendix/Supplementary material (Fig. A1). In the following, we analyze the clusters generated with a random data order by landslide ID.

The optimal number of 3 suitable clusters has been identified (Appendix/Supplementary material Fig. A2), with the help of the elbow plot, as explained in Sect. "Identification of landslide clusters", where an increase of *k* to four clusters did not result in a significant decrease of the sum of squared distances anymore.

Figure 12 shows the distribution of landslides within each cluster (a) and a plot of the minimum distance to rivers vs. the minimum distance to ridges with colours indicating the corresponding clusters. The dot sizes represent the ND categories (low, medium, and high). The "Min within polygons" landslide representations are used below for the quantitative analysis. Figure 13 shows the distribution of the landslide clusters on a map.

As Fig. 12 shows, cluster 1 contains 100 landslides (57%) that are close to rivers and ridges, cluster 2 contains 21 landslides (12%) that are located farther away from ridges but close to rivers, and cluster 3 contains 54 landslides (31%) that are close to ridges and farther away from rivers. Thus, shallow landslides with medium to high ND seem to cluster in the proximity of ridges (first 100 m) in dry conditions, with only a few exceptions. This suggests that they might be seismically induced. Cluster 3 is close to ridges and distant to rivers (Fig. 12b), impeding the clear distinction between seismic and climatic triggers. Cluster 2 is close to rivers, but more than 100 m away from ridges, revealing their probable climatic origin.

In total, 88% of the landslides initiated close to ridges (Fig. 10b), where the slope quickly becomes steep below a relatively 'flat' crest. This slope variation is a classical morphology change in volcanic deposits or gently dipping rock beddings as also highlighted by Whitford-Stark (1982) and Martí et al. (2018). Such morphologies are shaped by landslides and retrogressive erosion and thus the morphology could be an additional factor besides seismic activity to explain the large cluster of landslides close to ridges as demonstrated in Fig. 13b. In this regard, it should be noted that some of these hills identified as 'ridges' by the Topographic Position Index-based landform classification might not all be typical 'ridges' as they cover relatively large areas and not only the peaks or drainage divides. However, among those topographic heights there are also classical ridges like the one shown by the view in Fig. 4c and d, which could be marked by

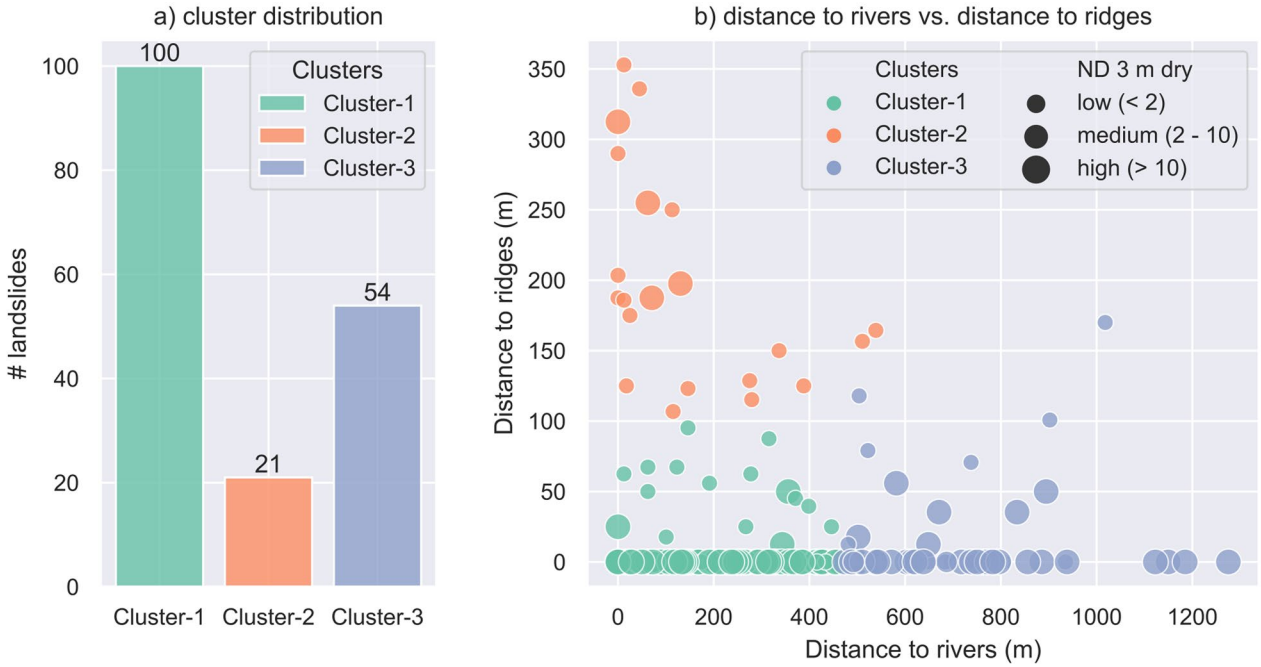

Fig. 12 Distribution of landslides within clusters (**a**) and minimum distance to rivers plotted against minimum distance to ridges for the minimum within landslide polygons with point sizes indicating Newmark displacement (**b**). The marker sizes represent the Newmark displacement ranges: low (< 2), medium (2–10) and high (> 10) values

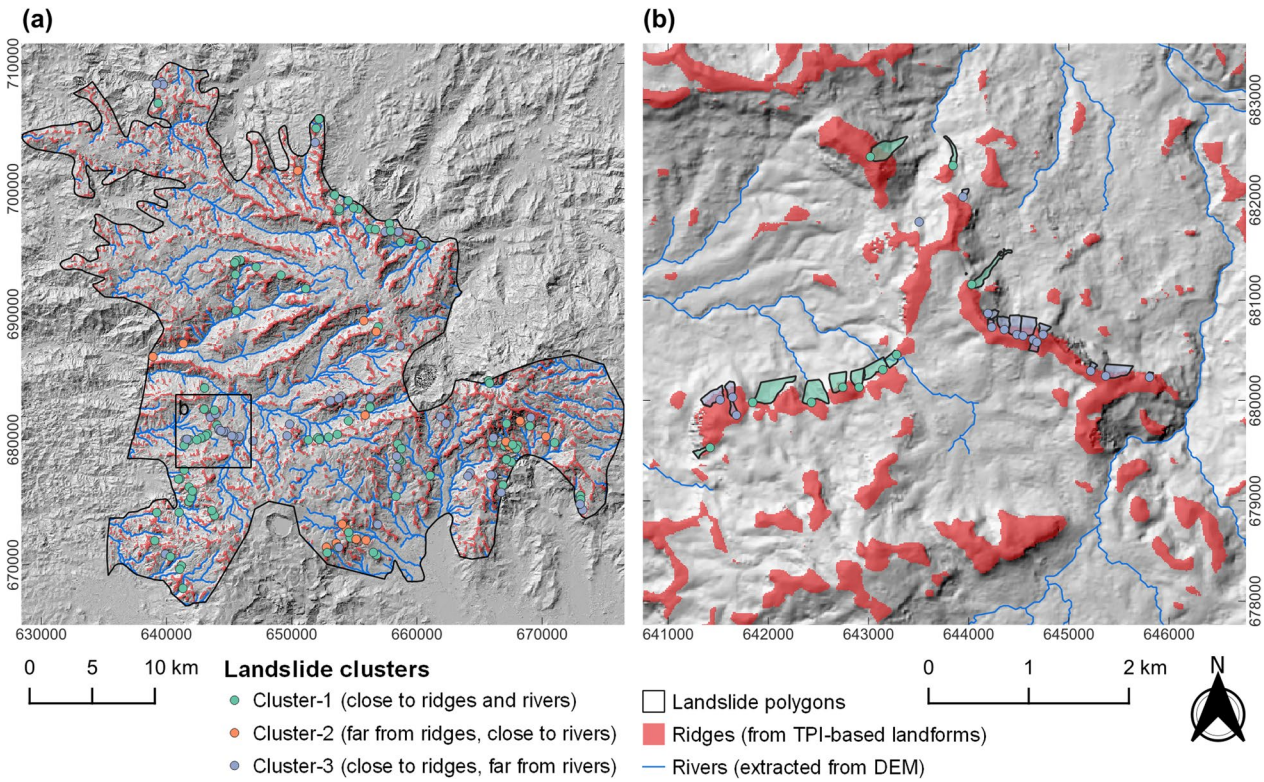

Fig. 13 Map with landslide clusters showing the ridges identified with the Topographic Position Index-based landforms tool and rivers extracted from the DEM (**a**) and zoomed-in view of landslides initiated along cuesta-like morphologies (**b**)

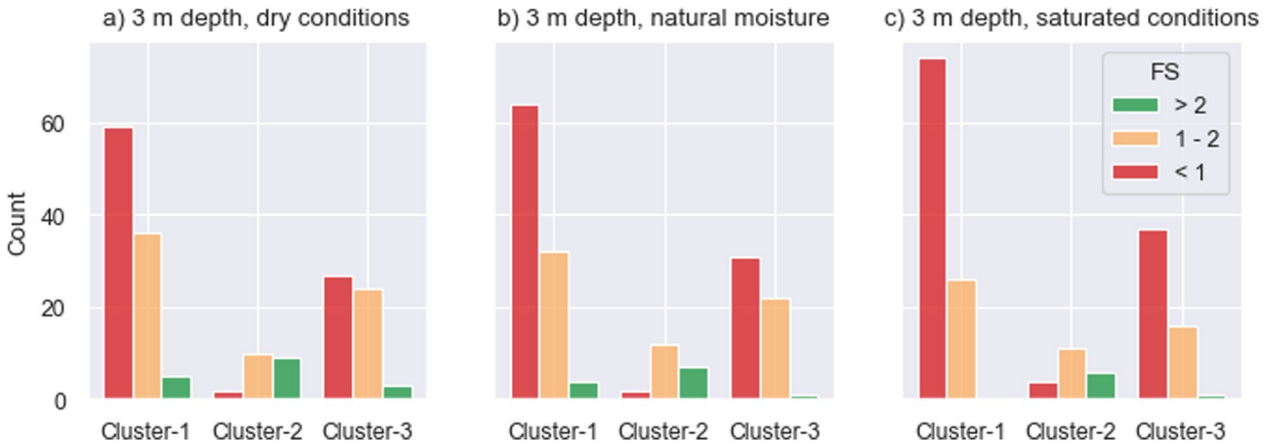

Fig. 14 Distribution of factor of safety stability domains over the three identified clusters for landslides at 3 m depth under dry (**a**), natural moisture (**b**), and saturated (**c**) conditions

some seismic amplification effects and related enhance slope instability (as highlighted, e.g., by Havenith et al. 2002; Mreyen et al. 2022).

We also analyzed the distribution of the stable, marginally stable, and instable FS domains over the three landslide clusters at 3 m depth and the three different saturation scenarios (Fig. 14). Clusters 1 and 3 show a high number of instable and marginally stable cases that increase with increasing water saturation. In contrast, the fraction of instable cases is low in cluster 2 (possible climatic origin), which is increasing only weakly with increasing saturation levels. This observation is a bit surprising, as especially for cluster 2, the landslides identified as likely climatically triggered respond only poorly to higher water saturation. At the same time, the clear response of some of the landslides close to ridges (clusters 1 and 3) indicates the influence of climatic factors. Cluster 2 seems to indicate a particular type of landslide occurring in more stable parts of the landscape.

Finally, we analyzed the distribution of the three ND domains (low, medium, high) over the three landslide clusters at 3 m depth under three water saturation levels (Fig. 15). Here cluster 2 shows generally mainly low ND values, while clusters 1 and 3 have a high proportion of landslides with very high ND values that are increasing with saturation levels, corresponding to the increase of the FS.

In summary, the cluster analysis did not provide sufficient insights to help discriminate between seismically- and climatically-induced landslide types. However, it helped reveal some insights into other factors characterizing specific landslide types, such as the vicinity to rather low ridges in the landscape. Cluster 1, with low FS and high ND values, makes sense for landslides near both ridges and rivers, as steep slopes under ridges and

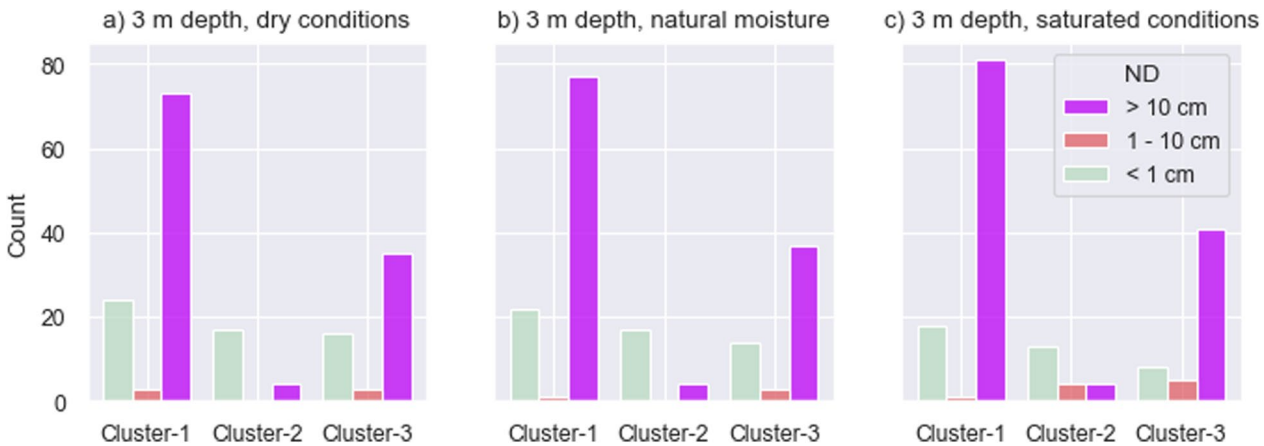

Fig. 15 Distribution of Newmark displacement (ND) domains over the three identified landslide clusters for landslides at 3 m depth under dry (**a**), natural moisture (**b**), and saturated (**c**) conditions

near rivers are more likely to be unstable (due to combined possible seismic effects near the crest and erosion of the toe by the river). Nevertheless, cluster 3 is the most interesting in favor of the seismic origin (as not affected by destabilization by a river) that could be further analyzed.

Conclusions

The landslide inventory mapped at the western flank of Mount Oku western part of the seismically active CVL revealed the presence of some landslides classified as spreads or complex landslides. These landslides indicate a sudden weakening of the soil, possibly caused by seismic activity or heavy rainfall leading to groundwater rise. Due to the lack of local seismic and corresponding landslide data, the role of earthquakes in triggering or preconditioning landslides in the Mount Oku area is not well understood. We proposed a framework for combining a deterministic geotechnical approach with statistics and k-means cluster analysis to investigate the contribution of earthquakes and rainfall on landslide development or reactivation in this region. We simulated the effect of a magnitude 5.2 earthquake, with an epicenter of 10 km from the area, on the stability of the western flank of Mount Oku slopes, assuming different failure depths and wetness conditions. Then, we first performed the qualitative analysis of the landslides' FS and ND, and a quantitative evaluation of the relationship between 179 shallow to deep landslides, and their distance to rivers and ridges using the cluster analysis. The results revealed that:

- Some landslide sites exhibit an FS less than 1 and high ND, characteristics associated with potential seismic-induced landslides. These locations could experience future landslides if an earthquake with a magnitude of 5.2, as assumed for these simulations, were to occur.
- Landslides with FS values between 1 and 2 and relatively high ND values (> 10 cm), already marginally stable, so that an additional destabilizing effects of an earthquake or a rainfall could push them over the threshold into instability, at least for the simulated earthquake or an even stronger or closer event.
- 31% of landslides showing medium to high ND values tend to cluster near ridges (cluster 3), suggesting their seismic origin. This clustering is a key characteristic commonly observed for landslides triggered by seismic activity when they are located far from any river. Moreover, cluster 2 is closer to rivers, revealing their probable climatic origin.

Thus, while climatic factors play an important role in the occurrence of landslides on the western flank of Mt. Oku, as evidenced by the 12% of landslides in Cluster 2 that occur closer to the river, seismic events may also contribute by either predisposing to landslide development or reactivating landslides in combination with climatic events.

These results are of great importance for establishing targeted measures aiming to reduce the impact of landslides by addressing both climatic and seismic factors. These measures include develop early warning systems that integrate both climatic and seismic data to provide timely alerts to local communities; raise awareness within the local communities that after heavy or extended rainfall or felt earthquakes there is a higher possibility for landslides; implement land-use planning and zoning regulations that consider the combined risks of climatic and seismic factors; and promote reforestation and the use of vegetative cover to stabilize slopes, which can help reduce the risk of landslides.

Supplementary Information

The online version contains supplementary material available at https://doi.org/10.1186/s40677-024-00297-2.

Additional file 1.

Acknowledgements
We are thankful to the German Aerospace Center (DLR), which kindly provided the TanDEM-X DEM used for this landslide-susceptibility investigation.

Author contributions
All authors contributed to the study conception and design. Conceptualization: W.D.L.D., A.B., X.F., A.S.L.W., T.M.F.-S., and H.-B.H.; Investigation: W.D.L.D., A.B., X.F., A.S.L.W., T.M.F.-S., and H.-B.H.; Methodology: W.D.L.D.; Supervision: A.B., X.F., T.M.F.-S., and H.-B.H.; Validation: A.B. and H.-B.H.; Visualization: W.D.L.D. and A.B.; Writing-original draft: W.D.L.D., A.B., and H.-B.H.; Writing-review & editing: W.D.L.D., A.B., X.F., and H.-B.H. All authors have read and agreed to the published version of the manuscript.

Funding
Open Access funding enabled and organized by Projekt DEAL. This research is financially supported by the National Science Fund for Distinguished Young Scholars of China (Grant 42125702), the Natural Science Foundation Sichuan Province (Grant 22NSFSC0029), the Tencent Foundation through the XPLORER PRIZE (Grant XPLORER-2022-1012).

Availability of data and materials
Relevant data is presented in the paper and in the appendix/supporting information.

Declarations

Competing interests
The authors declare no competing interests.

Author details
[1]State Key Laboratory of Geohazard Prevention and Geoenvironment Protection, Chengdu University of Technology, Chengdu 610059, China. [2]Department of Engineering Geology, Institute of Applied Geosciences, Technische Universität Berlin, Ernst-Reuter-Platz 1, 10587 Berlin, Germany. [3]Department of Earth Sciences, Faculty of Sciences, University of Dschang, Dschang, Cameroon. [4]Geology Department-B18, Georisk and Environment, Liege University, B-4000 Sart Tilman, Liège, Belgium.

Received: 13 June 2024 Accepted: 2 October 2024
Published online: 18 October 2024

References

Alkarkhi AFM and Alqaraghuli WAA (2020). Applied statistics for environmental science with R. ISBN 978-0-12-818622-0. https://doi.org/10.1016/C2018-0-04126-2

Alsubal S, Sapari N, Harahap ISH (2018) The rise of groundwater due to rainfall and the control of landslide by zero energy groundwater withdrawal system. Int J Eng Technol 7(2.29):921–926. https://doi.org/10.14419/ijet.v7i2.29.14284

Ambraseys NN, Adams RD (1986) Seismicity of West Africa. Ann Geophys 4:679–702. https://doi.org/10.4236/jhrss.2020.83018

Ateba B, Ntepe N, Ekodeck GE, Soba D, Fairhead JD (1992) The recent earthquakes of South Cameroon and their possible relationship with main Geological units of central Africa. J Afr Earth Sci 14:365–369. https://doi.org/10.1016/0899-5362(92)90040-J

Ayonghe SN, Mafany GF, Ntasin EB, Samalang P (1999) Seismically activated swarm of landslides, tension cracks, and a rockfall after heavy rainfall in Bafaka, Cameroon. Int J Nat Hazards 19:13–27. https://doi.org/10.1023/A:1008041205256

Ayonghe SN, Ntasin EB, Samalang P, Suh CE (2004) The June 27, 2001 landslides on volcanic cones in Limbe, Mount Cameroon, West Africa. J Afr Earth Sci 39:435–439. https://doi.org/10.1016/j.jafrearsci.2004.07.022

Bang HN, Miles LS, Gordon RD (2019) Disaster risk reduction in Cameroon: are contemporary disaster management frameworks accommodating the Sendai framework agenda 2030? Int J Disaster Risk Sci. https://doi.org/10.1007/s13753-019-00238-w

Bray JD (2007). Simplified Seismic Slope Displacement Procedures. In: Pitilakis KD (eds) Earthquake geotechnical engineering. Geotechnical, Geol. and Earthquake Eng., vol 6. Springer, Dordrecht

Chang KT, Chiang SH, Hsu ML (2007) Modeling typhoon and earthquake-induced landslides in a mountainous watershed using logistic regression. Geomorphology 89:335–347. https://doi.org/10.1016/j.geomorph.2006.12.011

Che VB, Kervyn M, Ernst GGJ, Trefois P, Ayonghe S, Jacobs P, Van Ranst E, Suh CE (2011) Systematic documentation of landslide events in Limbe area (Mt Cameroon Volcano, SW Cameroon): Geometry, controlling and triggering factors. Nat Hazards 59:47–74. https://doi.org/10.1007/s11069-011-9738-3

Cheunteu Fantah CA, Mezoue CA, Mouzong MP, Tokam KAP, Nouayou R, Nguiya S (2022) Mapping of major tectonic lineaments across Cameroon using potential feld data. Earth Planets Sp 74:59. https://doi.org/10.1186/s40623-022-01612-7

Crozier MJ (2005) Multiple-occurrence regional landslide events in New Zealand: hazard management issues. Landslides 2:247–256. https://doi.org/10.1007/s10346-005-0019-7

Delgado J, Rosa J, Peláez JA, Rodríguez-Peces MJ, Garrido J, Tsigé M (2020) On the applicability of available regression models for estimating Newmark displacements for low to moderate magnitude earthquakes. The case of the Betic Cordillera (S Spain). Eng Geol 274:105710. https://doi.org/10.1016/j.enggeo.2020.105710

Déruelle B, Ngounouno I, Demaiffe D (2007) The "Cameroon Hot line" (CHL): a unique example of active alkaline intraplate structure in both oceanic and continental lithospheres. Compte Rendu Géoscience 339:589–600. https://doi.org/10.1016/j.crte.2007.07.007

Djukem WDL, Braun A, Wouatong ASL, Guedjeo C, Dohmen K, Wotchoko P, Fernandez-Steeger TM, Havenith H-B (2020) Effect of soil geomechanical properties and geo-environmental factors on landslide predisposition at Mount Oku, Cameroon. Int J Environ Res Public Health 17:6795. https://doi.org/10.3390/ijerph17186795

Djukem WDL, Fan X, Braun A, Chevalier M-L, Wang X, Dai L, Fang C, Zhang X, Gorum T, Xu Q, Havenith H-B (2024) Traditional and modified Newmark displacement methods after the 2022 Ms 6.8 Luding earthquake (Eastern Tibetan Plateau). Landslides 21:807–828. https://doi.org/10.1007/s10346-023-02194-5

Doglioni A, Galeandro A, Simeone V (2013) Lateral strength and critical depth in infinite slope stability analysis. Int J Numer Anal Meth Geomech 38:1–9. https://doi.org/10.1002/nag.2190

Fitton JG (1980) The Benue Trough and Cameroon line-a migrating rift system in west Africa. Earth Planet Sci Lett 1:132–138. https://doi.org/10.1016/0012-821X(80)90261-7

Gountie DM, Nono A, Njonfang E, Kamgang P, Zangmo TG, Kagou DA, Nkouathio GD (2011) Dynamic and evolution of the Mounts Bamboutos and Bamenda calderas by study of ignimbritic deposits (West-Cameroon, Cameroon Line). Syllabus Rev Sci Ser 3:11–23

Havenith HB, Jongmans D, Faccioli E, Abdrakhmatov K, Bard PY (2002) Site effects analysis around the seismically induced Ananevo rockslide. Kyrgyzstan Bull Seis Soc Am 92(8):1–20. https://doi.org/10.1785/0120010206

Havenith H-B, Strom A, Caceres F, Pirard E (2006) Analysis of landslide susceptibility in the Suusamyr region, Tien Shan: statistical and geotechnical approach. Landslides 3:39–50. https://doi.org/10.1007/s10346-005-0005-0

Jibson RW (2007) Regression models for estimating co-seismic landslide displacement. Eng Geol 91(2):209–218. https://doi.org/10.1016/j.enggeo.2007.01.013

Jibson RW, Harp EL, Michael JA (1998) A method for producing digital probabilistic seismic landslide hazard maps: an example from Los Angeles, California Area. U.S. geological survey. Open File Rep. https://doi.org/10.1016/S0013-7952(00)00039-9

Jibson RW, Harp EL, Michael JA (2000) A method for producing digital probabilistic seismic landslide hazard maps. Eng Geol 58:271–289. https://doi.org/10.1016/S0013-7952(00)00039-9

Johari A, Javadi AA (2012) Reliability assessment of infinite slope stability using the jointly distributed random variables method. Sci Iranica A 19(3):423–429. https://doi.org/10.1016/j.scient.2012.04.006

Kamgang P, Njonfang E, Chazot G, Tchoua FM (2007) Géochimie et géochronologie des laves felsiques des Mounts Bamenda (ligne volcanique du Cameroun). C R Géoscience 339:659–666. https://doi.org/10.1016/j.crte.2007.07.011

Kamgang P, Njonfang E, Nono A, Gountie DM, Tchoua MF (2010) Petrogenesis of a silicic magma system: geochemical evidence from Bamenda Mountains, NW Cameroon, Cameroon volcanic line. J Afr Earth Sci 58:285–304. https://doi.org/10.1016/j.jafrearsci.2010.03.008

Keefer DK and Wilson RC (1989) Predicting earthquake-induced landslides, with emphasis on arid and semi-arid environments. In: Sadler and Morton (eds) Landslides in a Semi-arid environment, Inland Geological Society, 2: 118–149

Keles F, Nefeslioglu H (2021) Infinite slope stability model and steady-state hydrology-based shallow landslide susceptibility evaluations: the Guneysu catchment area (Rize, Turkey). CATENA 200:105161. https://doi.org/10.1016/j.catena.2021.105161

Kumar S, Gupta V, Kumar P, Sundriyal YP (2021) Coseismic landslide hazard assessment for the future scenario earthquakes in the Kumaun Himalaya, India. Bull Eng Geol Environ 80:5219–5235. https://doi.org/10.1007/s10064-021-02267-6

Martí J, Groppelli G, da Silveira AB (2018) Volcanic stratigraphy: a review. J Volcanol Geotherm Res. https://doi.org/10.1016/j.jvolgeores.2018.04.006

Marzoli A, Renne PR, Peccirillo EM, Castorina F, Bellieni G, Melfi AG, Nyobe JB, N'ni J (1999) Silicic magmas from the continental Cameroon Volcanic Line (Oku, Bambouto and Ngaoundere): 40Ar-39Ar dates, petrology, Sr-Nd-O isotopes and their petrogenetic significance. Contrib Miner Pet 135:133–150. https://doi.org/10.1007/s004100050502

Mfondoum AHN, Nguet PW, Seuwui DT et al (2023) Stepwise integration of analytical hierarchy process with machine learning algorithms for landslide, gully erosion and flash flood susceptibility mapping over the North-Moungo perimeter. Cameroon Geoenviron Disasters 10:22. https://doi.org/10.1186/s40677-023-00254-5

Miles SB, Ho CL (1999) Rigorous landslide hazard zonation using Newmark's method and stochastic ground motion simulation. Soil Dyn Earth Eng 18:305–323. https://doi.org/10.1016/S0267-7261(98)00048-7

Moreau C, Regnouit S-M, Deruehe B, Robinea B (1987) A new tectonic model for the Cameroun Line, Central Africa. Tectonophysics 139:317–334

Mreyen A, Donati D, Elmo D, Donze F, Havenith H (2022) Dynamic numerical modelling of co-seismic landslides using the 3D distinct element method: insights from the Balta rockslide (Romania). Eng Geol 307:106774. https://doi.org/10.1016/j.enggeo.2022.106774

Ndikum EN, Tabod CT, Tokam APK, Essimbi BZ (2014) Fault- Plane solution of the earthquake of 19 March 2005 in Monatele (Cameroon). Open J Geol 4:289–293. https://doi.org/10.4236/ojg.2014.46021

Newmark NM (1965) Effects of earthquakes on dams and embankments. Geotechnique 15(2):139–160. https://doi.org/10.1680/geot.1965.15.2.139
Ngapna MN, Owona S, Ateba CB, Mboudou GMM, Defo PLW (2022) The Western Cameroon highland margin: is there any geomorp hometric evidence of active tectonics? Geol J 57(29):60–2981. https://doi.org/10.1002/gj.4449
Ngatchou HE, Nguiya S, Owona Angue MLC, Mouzong PM, Tokam Kamga AP (2018) Source characterization and tectonic implications of the M4.6 Monatele (Cameroon) earthquake of 19 Marth (2005). S Afr J Geol 121(2):191–200. https://doi.org/10.25131/sajg.121.0015
Ngongang AW, Lenhardt N, Smit A (2018) Seismic hazard parameter estimation of the Mount Cameroon volcanic region (Cameroon) based on a combination of mixed catalogs. Nat Hazards 96:369–388. https://doi.org/10.1007/s11069-018-3547-x
Njilah K, Temdjima R, Richard C, Ghogomu N, Tchuitchou R, Ajonina H (2007) Geochemistry of tertiary-quaternary lavas of Mt. Oku Northwest Cameroon. Revista Facultad De Ingeniería 40:59–75
Nnange JM, Djallo S, Fairhead JD, Stuart GW (1983) Earthquake activity in Cameroon during 1983. Rev Sci Et Tech Ser Sci Terre 1:1–2
Nnange JM, Ngako VD, Fairhead J, Ebinger CJ (2000) Depths to density discontinuities beneath the Adamawa Plateau region, Central Africa, from spectral analysis of new and existing gravity data. J Afr Earth Sci 30(4):887–901. https://doi.org/10.1016/S0899-5362(00)00058-0
Ntepe N, Aka FT, Ubangoh RU, Ateba B, Nnange JM, Hell JV (2004) The July 2002 earthquake in the Kribi region: geological context and a preliminary evaluation of seismic risk in southwestern Cameroon. J Afr Earth Sci 40:163–172. https://doi.org/10.1016/j.jafrearsci.2004.09.002
Okimura T, Kawatani T (1986) Mapping of the potential surface-failure sites on granite mountain slopes. In: Gardiner V (ed) Int geomorp part I. Wiley, New York, pp 121–138
Qiu H, Su L, Tang B, Yang D, Ullah M, Zhu Y, Kamp U (2024) The effect of location and geometric properties of landslides caused by rainstorms and earthquakes. Earth Surf Proc Land. https://doi.org/10.1002/esp.5816
Rana K, Ozturk U, Malik N (2021) Landslide geometry reveals its trigger. Geophys Res Lett. https://doi.org/10.1029/2020gl090848
Rana K, Malik N, Ozturk U (2022) Landsifier v1.0: a Python library to estimate likely triggers of mapped landslides. Nat Hazard Earth Sys 22:3751–3764. https://doi.org/10.5194/nhess-22-3751-2022
Tabod CT, Fairhead JD, Stuart GW, Ateba B, Ntepe N (1992) Seismicity of the Cameroon Volcanic Line. 1982–1990. Tectonophysics 212:303–320. https://doi.org/10.1016/0040-1951(92)90297-J
Van Westen CJ (2004) Geo-information tools for landslide risk assessment: an overview of recent developments. Landslides Eval Stab 1:39–56. https://doi.org/10.1201/b16816-6
Venkatramanan S, Prasanna MV, Chung SY (2019) In GIS and geostatistical techniques for groundwater science. https://doi.org/10.1016/C2017-0-02667-8
Wendler T, Gröttrup S (2021) Data mining with SPSS modeler: theory, exercises and solutions. Springer
Whitford-Stark JL (1982) Factors influencing the morphology of volcanic landforms: an earth-moon comparison. Earth Sci Rev 18(2):1–168. https://doi.org/10.1016/0012-8252(82)90050-2
Woolley AR (2001) Oku. Alkaline rocks and carbonatites of the world, Part 3. Geological Society, p 35
Wotchoko P, Bardintzeff J-M, Itiga Z, Nkouathio DG, Guedjeo CS, Ngnoupeck G, Dongmo AK, Wandji P (2016) Geohazards (floods and landslides) in the Ndop Plain. Cameroon Volcanic Line Open Geosci 8:429–449. https://doi.org/10.1515/geo-2016-0030
Yuan RM, Deng QH, Dickson Cunningham ZJ, Han DL, Zhang B, Zhang BL (2016) Newmark displacement model for landslides induced by the 2013 Ms 7.0 Lushan earthquake, China. Front Earth Sci 10(4):740–750. https://doi.org/10.1007/s11707-015-0547-y
Zhang K, Peng X, Chen Y, Yan Y, Mei Q, Chen Y, Zhang D (2023) Cluster analysis of carboniferous gas reservoirs and application of recovery prediction model. Front Earth Sci 11:1220189. https://doi.org/10.3389/feart.2023.1220189

Publisher's Note